Snubber Branch Design and Development of Solid-State DC Circuit Breaker

Xin Yan, Zhanqing Yu, *Member, IEEE*, Lu Qu, *Member, IEEE*, Zhizheng Gan, Chunpin Ren, Jinpeng Wu, *Member, IEEE*, Jiapeng Liu, *Member, IEEE*, Rong Zeng, *Senior Member, IEEE*, and Yulong Huang, *Member, IEEE*

***Abstract*—This research proposes a solid-state dc circuit breaker for low voltage dc system based on reverse-blocking integrated gate-commutated thyristor (IGCT). The circuit breaker topology gets easier as a result of reverse-blocking IGCTs' ability to withstand reverse voltage. To further enhance the breaking process, we develop a snubber branch with metal oxide varistors (MOVs) and capacitance. The advantages and disadvantages of three distinct snubber branches—the no-snubber, the resistance–capacitance (*RC*), and the MOV-C snubber branch—are then contrasted. In addition to suppressing high-frequency oscillation caught by the parasitic MOV parameters, the structure with MOV-C snubber branch also blocks low-frequency harmonics brought on by *RC* snubber branch. Moreover, this structure can slow down the rate at which the voltage rises during the breaking process. Comparatively speaking to the *RC* snubber branch and no-snubber branch structures, it is more appropriate for solid-state dc circuit breakers. Finally, a solid-state dc circuit breaker prototype based on RB-IGCT and MOV-C branch has been created. The maximum overvoltage is 1.5 kV and the rated voltage is 750 V. The maximum breaking current is 10 kA and the rated current can be 2 kA.**

***Index Terms*—MOV-C structure, reverse-blocking integrated gate-commutated thyristor (IGCT), snubber branch, solid-state dc circuit breaker (SSCB).**

I. Introduction

FLEXIBLE power allocation, high system efficiency, high power supply capacity, minimal line loss, and high power quality are the advantages of the dc system [1], [2], [3], [4], [5], [6]. The short fault's effect on the current, however, manifests much more quickly in the dc system due to its low impedance [7], [8], [9]. Additionally, since dc fault current does not naturally have a zero-crossing point, cutting off the fault current is more difficult [10], [11]. Higher standards for the protection of the dc system have been proposed as a result of these challenges. With its great current-breaking capabilities and quick operating speed, the dc circuit breaker has provided the best performance for the short fault of a dc system. Solid-state dc circuit breakers (SSCBs), based on power electronic devices, have the advantages of a simplified structure, faster breaking speed, and no arc breaking as compared to mechanical dc circuit breakers (MCBs) and hybrid dc circuit breakers (HCBs). Moreover, SSCBs have a longer electrical life and greater dependability than the other two topologies due to the no arcing and moving structures [12], [13], [14]. The three topologies of dc circuit breakers are compared in Table I [1]. The SSCB has a comparatively low capital expenditure, but its operating cost is quite high due to the long-term loss. Although SSCBs have higher on-state losses

TABLE I
Characteristics Comparison of DCCB

		Mechanical	Hybrid	Solid-state
Breaking time		Long	Medium	Very short
Arc ablation		Serious	Ordinary	None
Control		Ordinary	Complex	Easy
Cost	Capex	Medium	High	Low
	Opex	Low	Medium	High
On-state loss		Low	Medium	High

TABLE II
Parameter of the Prototype

	A-IGCT (Abb-5SHY55L4500)	RB-IGCT (Peri-RBC52L3300)
Repetitive peak off-state voltage	4.5 kV	3.3 kV
Repetitive peak reverse voltage	0	3.3 kV
Controllable turn-off current	5 kA	5.2 kA
Max. peak non-repetitive surge on-state current at 3ms, 125°C	33 kA	27 kA
Critical rate of rise of on-state current	200 A/μs	200 A/μs
Threshold voltage	1.12 V	1.2 V
Slope resistance	0.28 mΩ	0.26 mΩ

Manuscript received 10 December 2022; revised 14 March 2023 and 17 April 2023; accepted 27 May 2023. Date of publication 31 May 2023; date of current version 1 September 2023. This work was supported in part by the National Natural Science Foundation of China under Grant 51922062 and in part by the Integration Projects of National Natural Science Foundation of ChinaState Grid Joint Fund for Smart Grid under Grant U2166602. Recommended for publication by Associate Editor F. Dijkhuizen. *(Corresponding author: Zhanqing Yu.)*

The authors are with the State Key Laboratory of Safety Control and Simulation of Power System and Large Power Generation Equipment, Tsinghua University, Beijing 100084, China (e-mail: yan-x19@mails.tsinghua.edu.cn; yzq@tsinghua.edu.cn; qulu@mail.tsinghua.edu.cn; ganzz20@mails.tsinghua.edu.cn; 18810903251@163.com; jinpengwu@tsinghua.edu.cn; liujiapeng@mail.tsinghua.edu.cn; zengrong@tsinghua.edu.cn; yulonghuang@tsinghua.edu.cn).

Color versions of one or more figures in this article are available at https://doi.org/10.1109/TPEL.2023.3281588.

Digital Object Identifier 10.1109/TPEL.2023.3281588

TABLE III
INFLUENCES OF C_S AND R_S ON THE VOLTAGE AND CURRENT DURING THE BREAKING PROCESS

Parameters	Effect on the voltage	Effect on the current
C_s	Reduce the overvoltage and the dv/dt	Reduce the speed of current commutation to the energy-absorbing MOV
R_s	Increase dv/dt but reduce the overvoltage	Speed up the current commutation

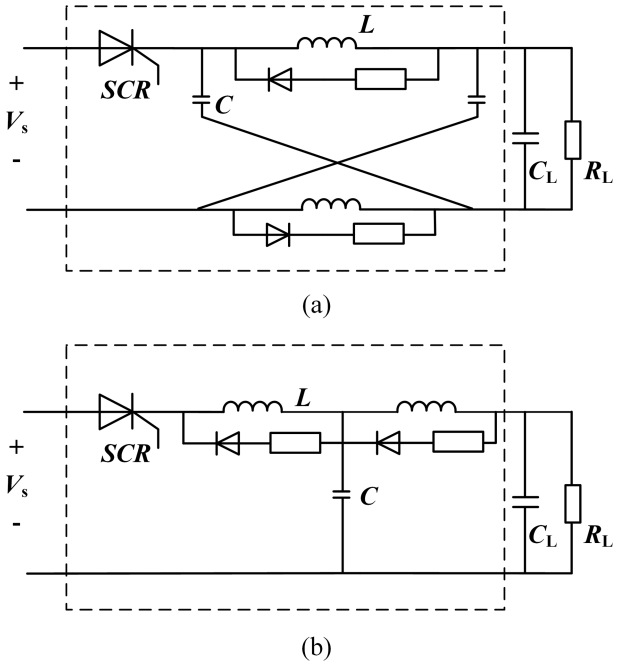

Fig. 1. Topologies of SSCB based on SCR. (a) Z-source breaker. (b) T-source breaker.

than MCBs and HCBs, their efficiency can exceed 99.5%, and current heat dissipation technology can guarantee the safety of the devices. Thus, SSCBs are frequently used in the data center, dc distribution network, and rail transit industries [15], [16], [17]. The rated current of the system is often between 1 and 2 kA in these low-voltage, high-capacity dc application circumstances. The fault current frequently reaches 10 kA within 1 ms, which need SSCB to isolate the short faults.

The most widely utilized high power electronic devices are the insulated gate bipolar transistor (IGBT), injection-enhanced gate transistor, and integrated gate-commutated thyristor (IGCT) [18], [19]. IGCT is more suited for SSCB since it has a low on-state voltage and can break greater fault currents after prolonged conduction. The employment of thyristors in SSCB is severely constrained even though they have a lower on-state voltage than IGCT. The Z-source and T-source SSCB topologies, which are depicted in Fig. 1, were proposed by many researchers, and are based on thyristors [20], [21]. However, compared to SSCBs based on full-controlled devices, topologies based on thyristors are typically more complex in structure and control and take longer time to break. Reverse-blocking IGCT (RB-IGCT) has been created as a result of technological advancements. With the

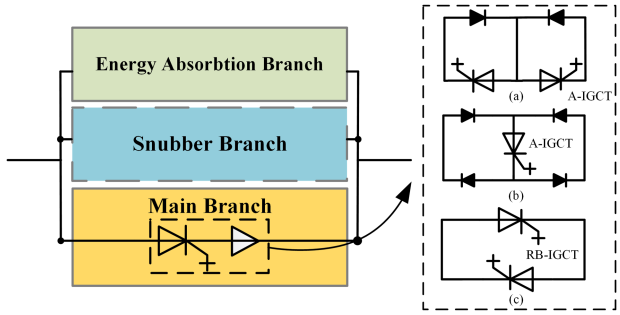

Fig. 2. Schematic of a typical SSCB with fully controlled power electronic devices.

ability to handle both forward and reverse voltage, RB-IGCT differs from asymmetric IGCT (A-IGCT) and reverse-conducting IGCT (RC-IGCT), simplifying SSCBs topology and control operations while reducing the price and size of circuit breakers [22].

A schematic of a typical SSCB is shown in Fig. 2. The main flow branch, the snubber branch, and the energy branch are the three branches that SSCBs typically have [23]. The main flow branch often consists of power electronics components, such as diodes, IGCTs, and IGBTs. In comparison to other structures using A-IGCT, the RB-IGCT structure employs less devices. The metal oxide varistor (MOV) is the main component of the energy branch. The snubber branch frequently uses a resistor–capacitor (*RC*) structure or a resistor–capacitor–diode structure to safeguard the devices and minimize stress during the dynamic operation. With more devices, the structure will get more complex and the dependability will drop due to the unidirectional conductivity of diodes and the crimping used to connect high-power diodes. Although the *RC* snubber structure is now the most popular, it has been discovered that if the load is a converter or the grid is highly volatile, this snubber branch cannot isolate periodic interference. The component, such as the snubber resistor, will become thermally damaged if there is constant current running through the *RC* snubber branch. So, the snubber branch requires a sensible setup to mitigate its drawbacks. We examined the effects of the three snubber configurations—no snubber branch, *RC* snubber branch, and MOV-C branch—each separately, weighing the benefits and drawbacks of each.

This study examines the benefits and drawbacks of various snubber branches and concludes that the MOV-C snubber method is the most effective option for SSCBs. The MOV-C structure's design approach and guiding principles are put out. In addition, an SSCB prototype built on the RB-IGCT and MOV-C snubber branch is developed. The structure of RB-IGCT and the SSCB work principle based on RB-IGCT are introduced in Section II. The effects of various snubber branches are compared in Section III, along with their benefits and drawbacks. The MOV-C structure offers clear advantages over the other two structures. A prototype SSCB with a MOV-C snubber branch that can resist 1.5 kV of excess voltage and turn OFF 10 kA of fault current is constructed in Section IV. Finally, Section V concludes this article.

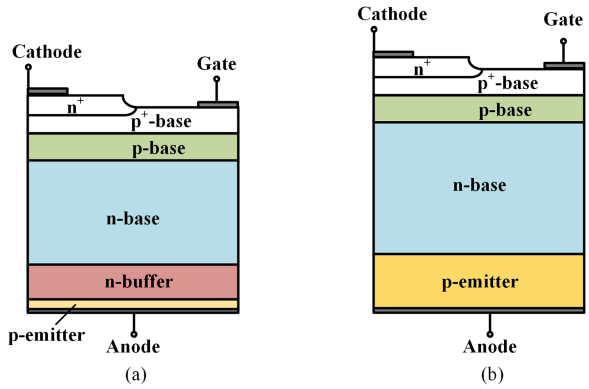

Fig. 3. Structure of different IGCT. (a) Asymmetric IGCT. (b) RB-IGCT.

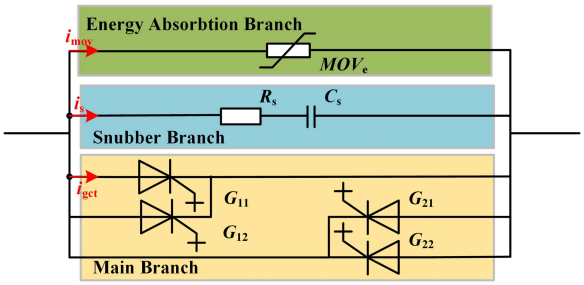

Fig. 4. Topology of SSCB based on RB-IGCT with *RC* snubber branch.

II. Solid-State Circuit Breaker Based on RB-IGCT

As illustrated in Fig. 3, RB-IGCT eliminates the n-buffer zone and thickens the p-base and n-base regions of the anode, enabling the J_1 junction to sustain reverse voltage. By varying the thickness and doping level of each area of the chip, RB-IGCT can have the same forward and reverse voltage. Because the main branch of the SSCB based on RB-IGCT is made up of reverse-parallel IGCT for bidirectional flow, the structure is simpler. Table II shows the typical parameter comparison between Asymmetric IGCT and RBIGCT.

The reverse-parallel construction has a lower on-state voltage and fewer power electronic components than more common main branch topologies, such as reverse-series and diode bridge, which lowers losses and costs. Three components typically make up the entire topology of an SSCB: the main branch, the snubber branch, and the energy branch. The major branch is made up of RB-IGCT, as shown in Fig. 4. The capacitor C_s and resistor R_s make up the snubber branch. An MOV is presented in the energy branch to control overvoltage and absorb system energy. In typical operation, the current flows via RB-IGCT on the main branch. In the event of a short-circuit malfunction, the control system sends an order to IGCT to turn OFF. The fault current is commutated to the snubber branch when IGCT turns OFF. The voltage of C_s grows as the snubber branch's current increases. The current is commutated from the snubber branch to the energy branch when the voltage across the snubber branch reaches the working voltage of the MOV. The system energy is absorbed by the MOV, and the fault current begins to fall. The process of breaking is finished when the voltage returns to the bus voltage. Fig. 5 shows the procedure for the SSCB to work. The long-term

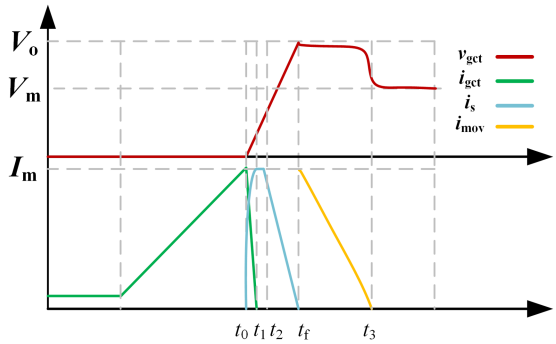

Fig. 5. Schematic diagram of the breaking waveform.

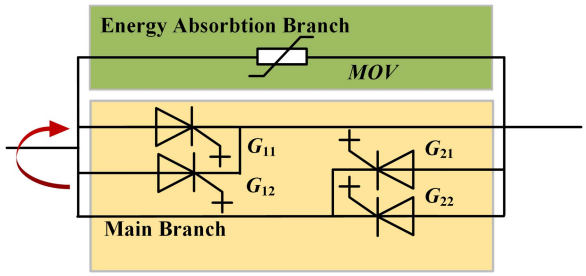

Fig. 6. Structure of SSCB without snubber branch.

rated voltage is V_m, whereas V_0 is the overvoltage. I_m refers to the highest turn-OFF current. I_{mov} and $I_{s,}$ respectively, stand for the energy absorption branch and snubber branch current.

III. Analysis of Structures With Different Snubber Branch

The breaking process is significantly impacted by the snubber branch. This section analyzes several snubber structures. They are contrasted in terms of both their benefits and drawbacks.

A. Structure Without Snubber Branch

The simplest straightforward approach is structure without snubber branch as shown in Fig. Fig. 6. This structure is more straightforward and convenient to design, which reduces volume of SSCBs. In addition, when the RB-IGCT is turned OFF, there is no snubber path for periodic leakage current and the bus voltage fluctuation is not sent to the load.

The residual MOV voltage during the breaking process is higher than the overvoltage of the structure without a snubber branch, though. On the one hand, when IGCT is turned OFF, the fault current is directly commutated from the main branch to the energy branch. The overvoltage will increase with high *di/dt* due to the MOV's steep front effect [24]. The voltage across the loop inductor between the main branch and the energy branch will rise, however, if the *di/dt* is high. Although the parallel MOV's residual voltage is 1.5 kV during the breaking test, the overvoltage reaches 2 kV, which is 25% more than the predicted value, as shown in Fig. 7. As a result, the utilization of power electrical devices without snubber branches will decrease because of the possibility of overvoltage failure if insufficient voltage margin is left.

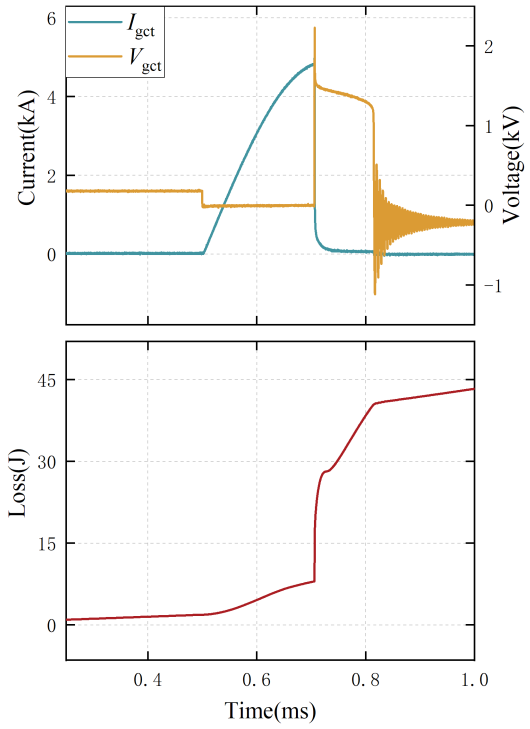

Fig. 7. Experiment result of the breaking process without snubber branch.

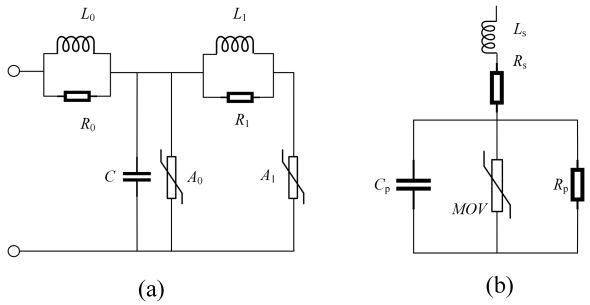

Fig. 8. MOV models. (a) Model of IEEE. (b) Model of Pspice.

The high-frequency oscillation of voltage is another issue. Through breaking trials, we discovered that the voltage of the IGCT oscillates at a high frequency at the conclusion of the breaking process, as illustrated in Fig. 7. The IGCT's electromagnetic environment will deteriorate due to the high-frequency oscillation, raising the risk of equipment failure. Besides, the loss will increase 10% with the high-frequency oscillation.

The parallel MOV can be thought of as a variable resistor with low resistance at high voltage and high resistance at low voltage. The MOV model provided by IEEE is depicted in Fig. 8(a), whereas the Pspice model is typically simplified to create Fig. 8(b) [26], [27]. The variable resistor is parallel with the parasitic capacitance C_p, which produces the high-frequency oscillation. In conjunction with the Pspice model, the parasitic capacitance C_p is the reason that causes the high-frequency oscillation. The MOV returns to its high-impedance condition after the breaking process is complete. Along with the bus capacitance and inductance, the parallel parasitic capacitance will cause high-frequency oscillation. The stray inductance can

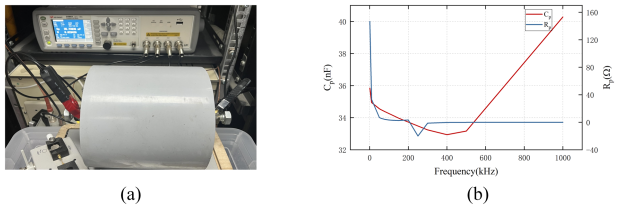

Fig. 9. MOV parameter analysis. (a) MOV sample and DA4980 instrument. (b) Result of parasitic parameter.

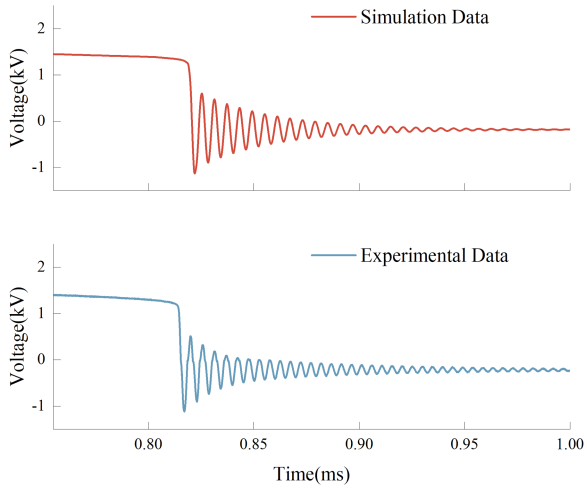

Fig. 10. Simulation waveforms and experimental waveforms considering the parasitic parameters of MOV.

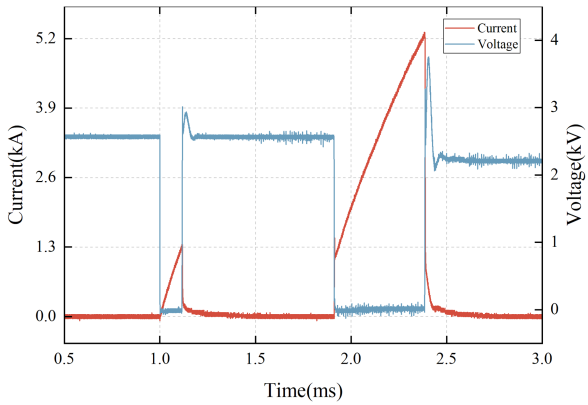

Fig. 11. Double-pulse turn-OFF experiment of IGCT.

be disregarded in the simplified model since it is negligibly small in comparison to the loop inductance.

We measure the energy-absorbing MOV with the Keysight DA4980 instrument in order to obtain the parasitic parameter of MOV. The experiment platform and results are displayed in Fig. 9. A resistor with 2.9 k and a capacitor with 34 nF are paralleled to create an identical MOV model in PSCAD, and the simulation results reveal that the oscillation's frequency and amplitude are comparable to those of the experiment, as shown in Fig. 10. The two voltage waveforms are very similar so that our hypothesis can be validated. We added to the double-pulse test without MOV in order to rule out the device's influence. Fig. 11 displays the examination outcomes. When the IGCT is

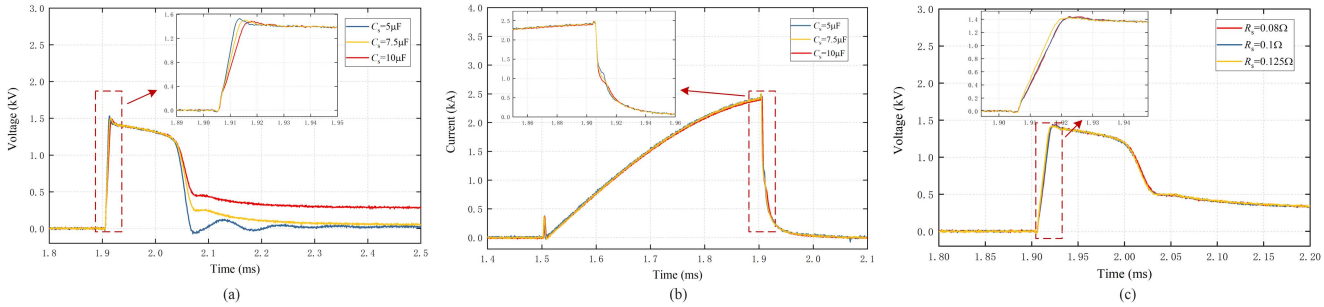

Fig. 12. Influence of R_s and C_s on the breaking process. (a) Influence of C_s on voltage. (b) Influence of C_s on current. (c) Influence of R_s on voltage.

turned OFF, there are no high-frequency oscillations in the voltage, which verifies the validity of the MOV model and validates the conclusion that the high frequent oscillation is caused by the MOV is right.

Although a structure without a snubber branch has some advantages, its main drawbacks are a substantially higher overvoltage and high-frequency voltage oscillation, reducing the security of breaking process.

B. *Structure With* RC *Snubber Branch*

The most popular method for limiting overvoltage is the *RC* snubber branch. Fig. 4 depicts the structure of the SSCB with the *RC* snubber branch. Since the voltage of C_s cannot change instantly, the snubber capacitor C_s will constrain the *dv*/*dt* during the breaking process, which also decrease the *di*/*dt* of the energy branch.

The capacitance of C_s should be as high as possible because of the steep front impact of MOV [24], [25]. t_f is the crucial moment for the MOV's steep front effect to manifest, and t_0 marks the beginning of the breaking process. The following equation can be obtained:

$$C_s U_{\max} = \int_{t_0}^{t_f} I dt. \tag{1}$$

$U_{\max}$ is the highest voltage that can be applied while breaking. I represents the current on the snubber branch. Assume that current can reach fault current $I_{\max}$ and that the current wave is a triangle, as illustrated in Fig. 5. The following expression is possible:

$$C_s = \frac{1}{2}\frac{I_{\max}(t_f - t_0)}{U_{\max}}. \tag{2}$$

Hence, the value of C_s should be greater than the value in (2).

When IGCT is turned ON, R_s is employed to restrict the surging current. The voltage across R_s during the breaking process must not, however, be higher than the IGCT's maximum voltage. The voltage will be lower than U_{main}, the IGCT maximum long-term sustain voltage, when IGCT is turned OFF. C_s will discharge through the IGCT if the IGCT is turned ON, and the current should be less than the IGCT's maximum surging current I_{surge}. Moreover, the voltage across the snubber resistance during the turn-OFF procedure needs to be lower than the IGCT maximum withstand voltage $U_{\max}$

$$\frac{U_{\text{main}}}{I_{\text{surge}}} \le R_s \le \frac{U_{\max}}{I_{\max}}. \tag{3}$$

R_s and C_s both have an impact on the breaking process. The capacitance of C_s affects voltage and current at the same amounts of voltage and current. To prevent overvoltage, an energy MOV with a 1.5-kV residual voltage is paralleled with an IGCT. According to Fig. 12(a), the smaller the value of C_s, the higher the *dv*/*dt* and the overvoltage. The effect of C_s on the fault current with 0.1-Ω snubber resistance is depicted in Fig. 12(b). Different snubber capacitances will affect how quickly the current declines, but eventually the current will converge. The current is diverted to the energy-absorbing branch more quickly the lower the capacitance. As a result, there will be a turning point in the currents, which is a sign that the current has switched to the energy branch. The effect of R_s when the snubber capacitance is 10 μF is shown in Fig. 12(c). With the lesser resistance, the voltage will be larger throughout the breaking process. The voltage of C_s will be lower when the voltage of R_s is high, even though the bigger resistance will have a higher voltage drop with the same current. The peak voltage is determined by the voltage of C_s thanks to a progressive reduction in the current in the snubber branch. Since the fault current is already commutated to MOV with a larger resistance, the voltage of C_s will be reduced. As a result, the peak voltage decreases while the *dv*/*dt* increases with increasing snubber resistance. Table V shows the influences of C_s and R_s on the voltage and current during the breaking process.

Even though the *RC* snubber branch can reduce the pace at which the voltage rises and the overvoltage, this branch will oscillate due to C_s and system inductance, as shown in Fig. 13. Because R_s has a low value, the oscillation cannot be effectively suppressed. On the one hand, this oscillation increases the voltage of the dc bus, potentially damaging the load. The *RC* snubber branch, on the other hand, offers a channel for periodic harmonics, and R_s will burn out as a result of persistent current flow. The following equation can be used to determine the oscillation frequency:

$$f = \frac{1}{2\pi\sqrt{LC}} = \frac{\sqrt{C_m + C_s}}{2\pi\sqrt{L_m C_m C_s}}. \tag{4}$$

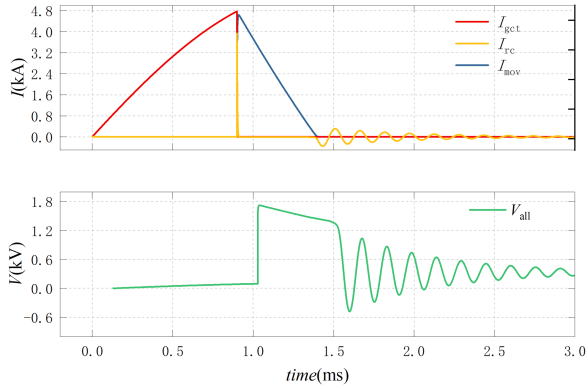

Fig. 13. Simulation waveform of the breaking process with *RC* snubber branch.

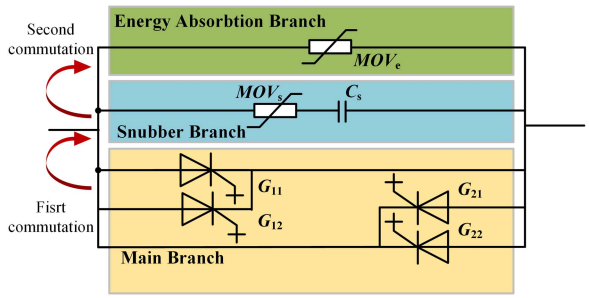

Fig. 14. Structure of SSCB with MOV-C snubber branch.

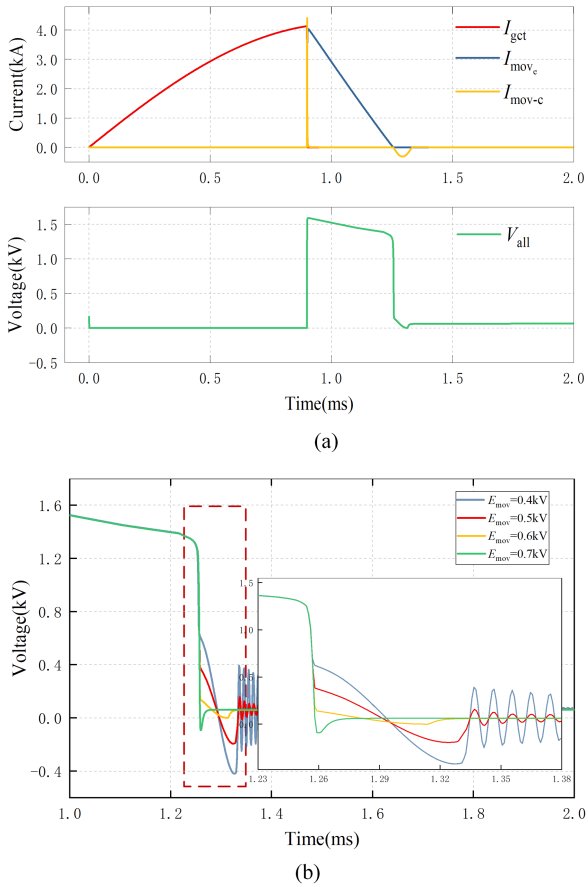

Fig. 15. Simulation results. (a) Breaking waveform of MOV-C snubber branch. (b) Influence of MOVs on breaking voltage.

L_m and C_m represent the bus inductance and the bus capacitor, respectively. In the experiment and simulation, the inductance of L_m is 66 μH and the capacitance of C_m is 4 mF. Considering the capacitance of C_s is 10 μF, the oscillation frequency is 6.2 kHz. The result is shown in Fig. 14.

C. Structure With MOV-C Snubber Branch

To resolve the issues with the aforementioned two topologies, a snubber branch of the MOV-C structure is suggested, as shown in Fig. 14. MOV_s and C_s combine to generate the snubber branch. After they are turned OFF, the voltage of the IGCT is gradually established. C_s will not be charged right away at the start of the breaking process because of MOV_s. The fault current is commutated from the main branch to the snubber branch and charges C_s to increase the voltage across the snubber branch when the voltage across IGCT is higher than the operating voltage of MOV_s. When the voltage across the snubber branch reaches the operational voltage of the MOV_e, the current is then commutated to the energy branch. When all of the system's energy is absorbed by MOV_e, the breaking process is completed.

The *dv*/*dt* and overvoltage during the breaking process can be decreased by the capacitor C_s on the snubber branch. When the oscillation voltage is lower than the operational voltage of MOV_s, the MOV_s can prevent ac leakage current and suppress the high-frequency oscillation brought on by the parasitic capacitance of MOV_e.

Because of MOV_s, the voltage of C_s during the breaking process is

$$U_c = \frac{U_{re}}{n} - U_s. \tag{5}$$

U_c is the voltage of C_s. U_{re} is the residual voltage of MOV_e. U_s is the rated voltage of MOV_s and n represents the number of series devices. When the voltage across MOV_e decreases to U_{sc}, C_s will discharge through MOV_s. We can get the expression of U_{sc}

$$U_{sc} = \frac{U_{re}}{n} - 2U_s. \tag{6}$$

With PSCAD/EMTDC, we model the structure using the MOV-C snubber branch. The outcomes are displayed in Fig. 15. E_{mov} refers to a MOV's rated voltage. Both the low-frequency and high-frequency oscillations are subdued. MOV_e's residual voltage is 1.5 kV. MOVs' rated voltage is 60% lower than MOV_e's. The effect of the MOV_s' voltage on the breaking voltage is depicted in Fig. 14(b). The voltage at which C_s discharges is lower and the oscillation's amplitude is decreasing as the rated voltage of MOV_s rises.

When the energy branch receives the fault current, the voltage will keep at the residual voltage of MOV_e. Once the energy of the system is absorbed by MOV_e, the overvoltage starts to decrease. The MOV-C snubber branch can muffle high-frequency MOV

TABLE IV
COMPARISON OF DIFFERENT SNUBBER STRUCTURES

Structure type	Cost	high frequency oscillation	low frequency oscillation	Overvoltage level
No snubber branch	Low	Yes	No	High
RC snubber branch	Medium	No	Yes	Low
MOV-C snubber branch	High	No	No	Medium

oscillations. The snubber branch will come back on as soon as the voltage of the MOV_e drops to U_{sc}. Because the resistance of MOV_s will be low and the capacitance of C_s will be considerably higher than that of C_p of MOV_e, C_s will discharge and inhibit the effect of the parasitic capacitance of MOV_e. MOV_s return to a high-resistance condition when the voltage of C_s drops to a low value, and a high-frequency oscillation will resurface, as shown in Fig. 15(b). The oscillation's amplitude is considerably lower than in topologies without a snubber branch, though, because the oscillation's beginning amplitude has been controlled.

The MOV-C snubber-equipped structure in certain ways makes structural design more challenging. Yet, the suppression of the oscillations and the overvoltage during the breaking process are both extremely noticeable. The comparison of the various SSCB snubber structures is shown in Table IV. The structure with a MOV-C branch is better suited for SSCB, per the analysis earlier.

The rated voltage, the residual voltage, and associated current, as well as absorbable energy, are the four main MOV parameters. To prevent increased current flow through the energy-absorbing MOV_e, when it is in the blocking condition, the rated voltage for the device can be 1.1 times the system bus voltage. The symbol α stands for the residual voltage to MOV rated voltage ratio. The resulting current should be the maximum breaking current of the SSCB, and the residual voltage should be 1.1α times greater than the bus voltage. The maximum breaking current and busbar inductance both affect how much energy MOV_e can hold at once. In addition, it is important to consider the energy of reclosing.

The voltage of C_s will be U_{rs}-U_s after IGCT is turned OFF. When IGCT is turned ON, MOV_s withstand the voltage of C_s. So, the residual voltage of MOV_s should be higher than the voltage of C_s. And the corresponding current should be the breaking current. The rated voltage of MOV_s can be calculated by U_{rs} and α_e. The energy of MOV_s at a single time can be described by (7). As with MOV_e, the energy of MOV_s during the reclosing process needs to be considered

$$E = \int_{t_0}^{t_f} u_s \cdot i_s dt \le U_{rs} I_{max}(t_f - t_0). \tag{7}$$

So, the vital parameters of MOV_e and MOV_s can be designed according to (8) and (9)

$$\begin{Bmatrix} U_e = 1.1U_{bus} \\ U_{re} = 1.1\alpha_e U_{bus} \\ I_{re} = I_{max} \\ E \ge LI_{max}^2 \end{Bmatrix} \tag{8}$$

TABLE V
PARAMETER OF THE PROTOTYPE

	Components	Parameters
Main branch	RB-IGCT	Peri RB52QY3300
Snubber branch	C_s	10 μF
	MOV_s	0.4 kV at 1 mA; 0.7 kV at 10 kA
Energy branch	MOV_e	1 kV at 1 mA; 1.5 kV at 10 kA

TABLE VI
RESULTS OF THE TEST

Index	Parameters
Rated Voltage	750 V
Max Overvoltage	1.5 kV
Maximum Controllable Turn-off Current	10 kA
Current Imbalance	4%
Max On-state Current	2 kA

$$\begin{Bmatrix} U_{rs} = \frac{U_{re}}{n(1+\alpha_s)} = \frac{1.1\alpha_e U_{bus}}{n(1+\alpha_s)} \\ U_s = \frac{U_{rs}}{\alpha_s} \\ I_{re} = I_{max} \\ E \ge 2U_{rs} I_{max}(t_f - t_0) \end{Bmatrix} \tag{9}$$

n represents the number of MOV_s.

The design of the value of C_s can be the same with the design of C_s in *RC* snubber branch.

IV. PROTOTYPE DESIGN AND EXPERIMENTAL RESULT

An SSCB prototype built on the RB-IGCT is created, and the experiment is run. The prototype's rated voltage is 750 V, and throughout the breaking process, there will be a 1500-V overvoltage. The maximum breaking current is 10 kA to meet the needs of most application scenarios, which can be realized by connecting two IGCTs in parallel. The component parameters are displayed in Table V.

A. Prototype and Test Platform

The prototype uses the MOV-C structure topology depicted in Fig. 14. To stop the 10-kA fault current, two Peri RB52QY3300 RB-IGCTs are connected in parallel. The primary branch for the bidirectional flow is made up of two additional RB-IGCTs that are reverse-parallel. In the snubber branch, MOV-C is present. The capacitance of C_s is 10 μF, whereas the residual voltage of MOV_s is 0.7 kV. The MOV_e, which has a 1.5-kV residual voltage, is the energy branch. This prototype's forced air-cooling system is based on gravity heat pipes. This approach does not need any

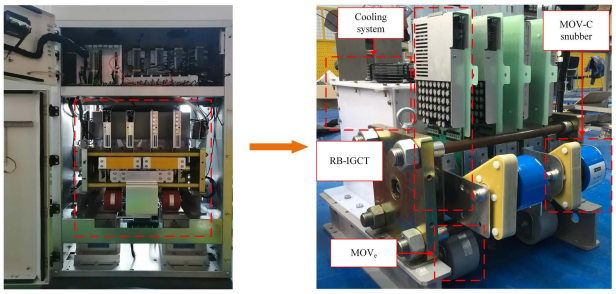

Fig. 16. Prototype of SSCB with MOV-C structure.

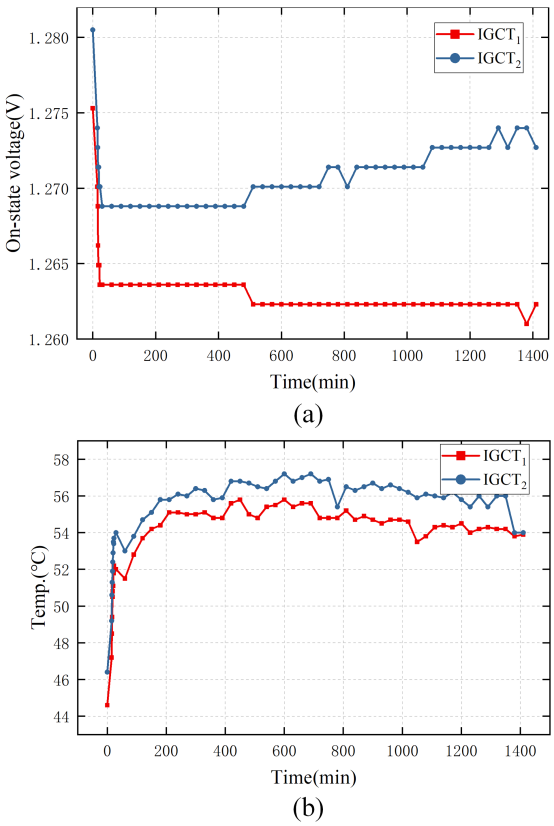

Fig. 17. Long-term working test result. (a) ON-stage voltage. (b) Temperature of heat sink.

additional equipment and can meet the heat dissipation requirement. Coolant is housed in the radiator's hollow chamber. While SSCB operates, the coolant absorbs and evaporates the heat produced by IGCT. The fan cools the coolant steam, which then condenses back. In order to achieve dependable heat dissipation of the SSCB, the evaporation and backflow of the coolant must likewise attain a dynamic equilibrium when the heat dissipation and generation do. The innovative SSCB's general structure is depicted in Fig. 16.

B. Test of SSCB

1) Long-Term Current Test: A long-term current test was done to check the SSCB's ability to dissipate heat during normal operation. The findings are presented in Fig. 17. The conduction

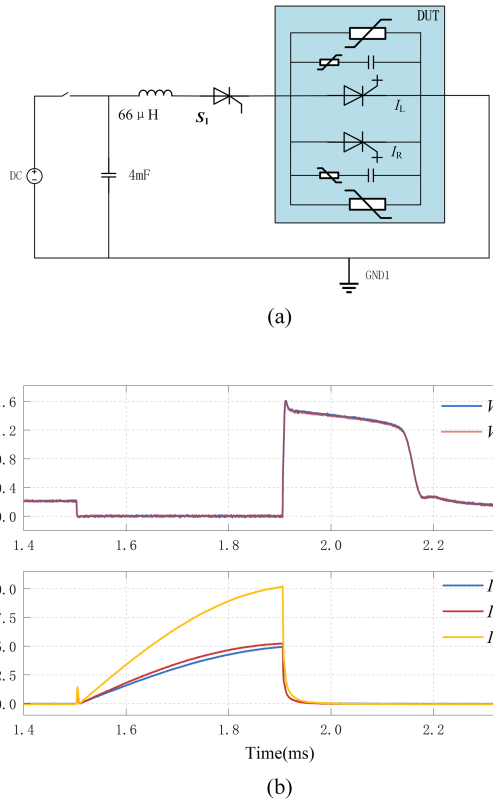

Fig. 18. 10-kA breaking test waveform with MOV-C snubber design. (a) Test circuit diagram. (b) Result of test.

voltage drops of two parallel RB-IGCTs linked to a 2-kA rated current are 1.26 and 1.27 V, respectively. At 56 °C and 54 °C, the heat sink surface's temperature is steady. 25 °C is the test environment temperature. As a result, the need is met by controlling the temperature rise of the gravity heat pipe to within 30 °C and the junction temperature of both operating IGCTs to within 70 °C under a 1-kW power consumption.

2) Breaking Test: To test the SSCB's ability to break, we performed the breaking experiment. In Fig. 18, the test waveforms are displayed. The IGCTs are turned ON and the current starts to climb at $t = 1.4$ ms, simulating a short fault. The paralleled IGCTs turn OFF at 4.8 and 5.2 kA, respectively, at $t = 1.9$ ms. The current is within 10% of becoming uneven. The residual voltage and the overvoltage are both capped by MOV_e, at 1.5 kV. Also, the oscillation is clearly suppressed, demonstrating that the topology with the MOV-C snubber may successfully address the oscillation issue.

We initially screen out IGCTs with consistent *I–V* characteristics and use them as parallel devices in order to increase the current uniformity. The valve's structural layout is also very symmetrical to minimize the effects of stray inductance variations, and the busbar has various connecting interfaces so that the features of parallel current sharing can be modified. In order to assure the consistency of the current sharing of the devices in parallel, we finally eliminated the effect of response delay time by changing the break time of the parallel devices.

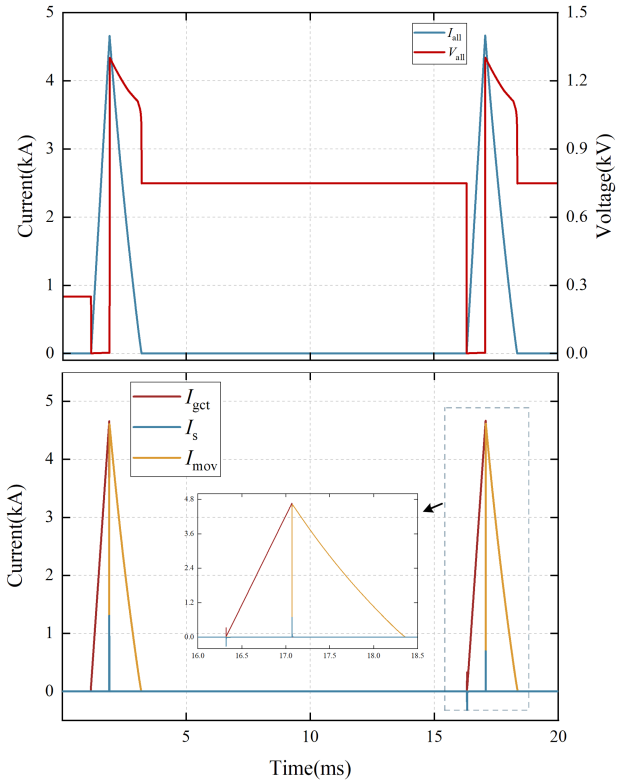

Fig. 19. Waveforms of OCO operation.

The outcomes of the open–close–open (OCO) process are displayed in Fig. 19. As can be observed, the RB-IGCT device and the MOV-C snubber branch enable the SSCB to effectively complete the OCO procedure. Table VI summarizes the test results.

V. Conclusion

This work investigates a large-capacity SSCB with an antiparallel construction based on the RB-IGCT. The impact of the snubber branches is analyzed. In the beginning, we examine the structure without snubber branches. During the breaking process, high-frequency voltage oscillation will be caused by the MOV's parasitic characteristics. The impact of the *RC* snubber branch and the influence of the *RC* parameters are then examined in relation to the breaking process. The main issues with this construction are its inability to suppress the ac component and low-frequency oscillations during turn-OFF process. We suggest the MOV-C snubber branch and have confirmed its inhibiting effect on the oscillating voltage as a solution to the problem of the two structures mentioned earlier. Also, the impact of the snubber MOV is examined, and a method for choosing the MOV parameters is suggested.

Ultimately, we created a prototype SSCB with a 750-V working voltage and a 2-kA working current. 10 kA is the maximum breaking current. Both the breaking test and the long-term flow test were successful, demonstrating the viability of the plan.

References

[1] W. Chen et al., "Development and prospect of direct-current circuit breaker in China," *High Voltage*, vol. 6, no. 1, pp. 1–15, Dec. 2020.

[2] C. Meyer, M. Kowal, and R. W. De Doncker, "Circuit breaker concepts for future high-power DC-applications," in *Proc. 40th IAS Annu. Meeting Conf. Rec. Ind. Appl. Conf.*, 2005, vol. 2, pp. 860–866.

[3] L. Qi et al., "Solid-state circuit breaker protection for DC shipboard power systems: Breaker design, protection scheme, validation testing," *IEEE Trans. Ind. Appl.*, vol. 56, no. 2, pp. 952–960, Mar./Apr. 2020, doi: 10.1109/TIA.2019.2962762.

[4] R. Rodrigues, Y. Du, A. Antoniazzi, and P. Cairoli, "A review of solid-state circuit breakers," *IEEE Trans. Power Electron.*, vol. 36, no. 1, pp. 364–377, Jan. 2021, doi: 10.1109/TPEL.2020.3003358.

[5] D. Marroquí, J. M. Blanes, A. Garrigós, and R. Gutiérrez, "Self-powered 380 V DC SiC solid-state circuit breaker and fault current limiter," *IEEE Trans. Power Electron.*, vol. 34, no. 10, pp. 9600–9608, Oct. 2019, doi: 10.1109/TPEL.2019.2893104.

[6] P. Cairoli, R. Rodrigues, U. Raheja, Y. Zhang, L. Raciti, and A. Antoniazzi, "High current solid-state circuit breaker for safe, high efficiency DC systems in marine applications," in *Proc. IEEE Transp. Electrific. Conf. Expo*, 2020, pp. 936–941, doi: 10.1109/ITEC48692.2020.9161515.

[7] Z. Dongye, L. Qi, X. Cui, P. Qiu, and F. Lu, "A new approach to model reverse recovery process of a thyristor for HVDC circuit breaker testing," *IEEE Trans. Power Electron.*, vol. 36, no. 2, pp. 1591–1601, Feb. 2021, doi: 10.1109/TPEL.2020.3007660.

[8] Z. Zhou, M. Chen, J. Jiang, D. Zhang, S. Ye, and C. Liu, "Analysis and design of a novel thyristor-based circuit breaker for DC microgrids," *IEEE Trans. Power Electron.*, vol. 35, no. 3, pp. 2959–2968, Mar. 2020, doi: 10.1109/TPEL.2019.2926581.

[9] Z. J. Shen, "Ultrafast solid-state circuit breakers: Protecting converter-based AC and DC microgrids against short circuit faults [Technology Leaders]," *IEEE Electrific. Mag.*, vol. 4, no. 2, pp. 72–70, Jun. 2016, doi: 10.1109/MELE.2016.2544058.

[10] D. Jovcic and B. Wu, "Fast fault current interruption on high-power DC networks," in *Proc. IEEE PES Gen. Meeting*, 2010, pp. 1–6, doi: 10.1109/PES.2010.5589953.

[11] C. M. Franck, "HVDC circuit breakers: A review identifying future research needs," *IEEE Trans. Power Del.*, vol. 26, no. 2, pp. 998–1007, Apr. 2011, doi: 10.1109/TPWRD.2010.2095889.

[12] G. B. De Lange, A. M. Chol, and N. M. Ijumba, "Application of high-power semiconductor technology in DC traction circuitbreakers," in *Proc. IEEE Power Eng. Soc. Inaugural Conf. Expo. Afr.*, 2005, pp. 494–498, doi: 10.1109/PESAFR.2005.1611872.

[13] K. Sano and M. Takasaki, "A surgeless solid-state DC circuit breaker for voltage-source-converter-based HVDC systems," *IEEE Trans. Ind. Appl.*, vol. 50, no. 4, pp. 2690–2699, Jul./Aug. 2014.

[14] R. Schmerda, R. Cuzner, R. Clark, D. Nowak, and S. Bunzel, "Shipboard solid-state protection: Overview and applications," *IEEE Electrific. Mag.*, vol. 1, no. 1, pp. 32–39, Sep. 2013.

[15] W. A. Martin, C. Deng, D. Fiddiansyah, and J. C. Balda, "Investigation of low-voltage solid-state DC breaker configurations for DC microgrid applications," in *Proc. IEEE Int. Telecommun. Energy Conf.*, 2016, pp. 1–6, doi: 10.1109/INTLEC.2016.7749139.

[16] G. D. Demetriades, W. Hermansson, J. R. Svensson, K. Papastergiou, and T. Larsson, "DC-breaker for a multi-megawatt battery energy storage system," in *Proc. Int. Power Electron. Conf. (IPEC-Hiroshima - ECCE ASIA)*, 2014, pp. 1220–1226, doi: 10.1109/IPEC.2014.6869742.

[17] D. Lawes, L. Ran, and Z. Xu, "Design of a solid-state D.C. circuit breaker for light rail transit power supply network," in *Proc. IEEE Energy Convers. Congr. Expo.*, 2014, pp. 350–357, doi: 10.1109/ECCE.2014.6953414.

[18] F. Agostini et al., "1MW bi-directional DC solid state circuit breaker based on air cooled reverse blocking-IGCT," in *Proc. IEEE Electric Ship Technol. Symp.*, 2015, pp. 287–292, doi: 10.1109/ESTS.2015.7157906.

[19] Z. Chen et al., "Analysis and experiments for IGBT, IEGT, and IGCT in hybrid DC circuit breaker," *IEEE Trans. Ind. Electron.*, vol. 65, no. 4, pp. 2883–2892, Apr. 2018.

[20] K. A. Corzine and R. W. Ashton, "Structure and analysis of the Z-source MVDC breaker," in *Proc. IEEE Electric Ship Technol. Symp.*, 2011, pp. 334–338, doi: 10.1109/ESTS.2011.577089.

[21] A. Overstreet, A. Maqsood, and K. Corzine, "Modified z-source DC circuit breaker topologies," in *Proc. Clemson Univ. Power Syst. Conf.*, 2014, pp. 1–6, doi: 10.1109/PSC.2014.6808121.

[22] U. Vemulapati et al., "Reverse blocking IGCT optimised for 1 kV DC bi-directional solid state circuit breaker," *IET Power Electron.*, vol. 12, no. 8, pp. 2308–2314, 2015.

[23] Q. Lu et al., "Design and analysis of a 375V/5kA solid state DC circuit breaker based on IGCT," in *Proc. IEEE Int. Power Electron. Appl. Conf. Expo.*, 2018, pp. 1–5, doi: 10.1109/PEAC.2018.8590635.

[24] X. Zhang, Z. Yu, Z. Chen, Y. Huang, B. Zhao, and R. Zeng, "Modular design methodology of DC breaker based on discrete metal oxide varistors with series power electronic devices for HVdc application," *IEEE Trans. Ind. Electron.*, vol. 66, no. 10, pp. 7653–7662, Oct. 2019, doi: 10.1109/TIE.2018.2886787.
[25] D. B. Miller, A. E. Lux, S. Grzybowski, and P. R Barnes, "The effects of steep-front, short-duration impulses on power distribution components," *IEEE Trans. Power Del.*, vol. 5, no. 2, pp. 708–715, Apr. 1990, doi: 10.1109/61.53073.
[26] IEEE Working Group 3. 4. 11, "Modeling of metal oxide surge arresters," *IEEE Trans. Power Del.*, vol. 7, no. 1, pp. 302–309, Jan. 1992.
[27] J. G. Zola, "Simple model of metal oxide varistor for Pspice simulation," *IEEE Trans. Comput.-Aided Des. Integr. Circuits Syst.*, vol. 23, no. 10, pp. 1491–1494, Oct. 2004, doi: 10.1109/TCAD.2004.835134.

Xin Yan was born in Chongqing, China, in 1997. He received the B.S. degree in electrical engineering in 2019 from Tsinghua University, Beijing, China, where he is currently working toward the Ph.D. degree in electrical engineering.

His current research interests include power semiconductor devices, dc circuit breaker, and HVdc system.

Zhanqing Yu (Member, IEEE) was born in Inner Mongolia, China, in 1981. He received the B.Sc. and Ph.D. degrees in electrical engineering from Tsinghua University, Beijing, China, in 2003 and 2008, respectively.

After graduation, he became a Postdoctor and Lecturer with the Department of Electrical Engineering, Tsinghua University, in July 2008 and July 2010, respectively, and an Associate Professor with the same department in December 2012. He has participated in several projects sponsored by High-Tech R&D Program (863 Program), National Basic Research Program of China (973 Program), and National Natural Science Foundation of China. His research interests include dc grid, dc breaker, electromagnetic environment and electromagnetic compatibility, and lightning protection.

Lu Qu (Member, IEEE) was born in 1987. He received the Ph.D. degree in electrical engineering from the University of Chinese Academy of Sciences, Hefei, China, in 2016.

He is currently an Associate Researcher with Tsinghua University, Beijing, China. He undertakes one China Postdoctoral Science Fund. He authored or coauthored 30 papers included in SCI /EI, authorized 25 invention patents, and applied for 40 invention patents. He participated in the preparation of five Chinese monographs and one English monograph. He also participated in drafting one national standard, three industrial standards, and three group standards. His research interests include dc grid and dc breaking technology.

Zhizheng Gan was born in Guangxi, China, in 1998. He received the B.S. degree in electrical engineering in 2020 from Tsinghua University, Beijing, China, where he is currently working toward the Ph.D. degree in electrical engineering.

His current research interests include mechanical switch, dc circuit breaker, and HVdc system.

Chunpin Ren was born in Zhejiang, China, in 1997. She received the B.S. degree in electrical engineering from the Department of Electrical Engineering, North China Electric Power University, Beijing, China, in 2019. She is currently working toward the Ph.D. degree in electrical engineering with the Department of Electrical Engineering, Tsinghua University, Beijing, China.

Her current research interests include high-power semiconductor device manufacturing, modeling, and development.

Jinpeng Wu (Member, IEEE) was born in Hebei, China, in 1987. He received the B.S. and Ph.D. degrees in electrical engineering from the Department of Electrical Engineering, Tsinghua University, Beijing, China, in 2010 and 2015, respectively.

From 2016 to 2020, he continued his research with Stanford University, Stanford, CA, USA, and Lawrence Berkeley National Laboratory, Berkeley, CA, USA, as a Postdoctoral Researcher. He is currently an Assistant Professor with the Department of Electrical Engineering, Tsinghua University. His research interests include the energy and electrical materials, power electronics, and X-ray spectroscopies.

Jiapeng Liu (Member, IEEE) was born in Liaoning, China, in 1994. He received the B.S. and Ph.D. degrees in electrical engineering from Tsinghua University, Beijing, China, in 2016 and 2021, respectively.

He is currently a ShuiMu Postdoctoral Researcher with Tsinghua University. His current research focuses on high-power semiconductor device fabricating, modeling, and development.

Rong Zeng (Senior Member, IEEE) was born in Shaanxi, China, in 1971. He received the B.Eng., M.Eng., and Ph.D. degrees in electrical engineering from the Department of Electrical Engineering, Tsinghua University, Beijing, China, in 1995, 1997, and 1999, respectively.

He was a Lecturer with the Department of Electrical Engineering, Tsinghua University, in 1999, and an Associate Professor and Professor with the same department in 2002 and 2007, respectively. He is currently working in the fields of air gap discharge, lightning protection, and electromagnetic compatibility in power systems, electric and magnetic field measurement by integrated electro-optical sensors, power semiconductor, HVdc system, and direct current circuit breaker.

Yulong Huang (Member, IEEE) was born in Hubei, China, in 1964. He received the B.Eng. degree in electrical engineering from Hunan University, Changsha, China, in 1985, and the M.Eng. degree in electrical engineering from Tsinghua University, Beijing, China, in 1991.

From 2000 to 2001, he was a Visiting Scholar with The University of Manchester (formerly UMIST), Manchester, U.K. He is currently an Associate Professor with the Department of Electrical Engineering, Tsinghua University, working on high-voltage circuit breakers and online monitoring for high-voltage equipment.